The Promise of Alloy Anodes for Solid-State Batteries

John A. Lewis[1], Kelsey A. Cavallaro[1], Yuhgene Liu[1], Matthew T. McDowell[1,2,3]*

[1] School of Materials Science and Engineering, Georgia Institute of Technology, Atlanta, GA, 30332, USA.

[2]George W. Woodruff School of Mechanical Engineering, Georgia Institute of Technology, Atlanta, GA, 30332, USA.

[3]Lead Contact

*Correspondence: mattmcdowell@gatech.edu

SUMMARY

Solid-state batteries are a next-generation technology that could feature improved safety and energy density, but reliably integrating high-capacity electrode materials to enable high energy while retaining stable long-term cycling remains a challenge. Anode materials that alloy with lithium, such as silicon, tin, and aluminum, offer high capacity that can yield high-energy battery cells. The use of alloy anodes in solid-state batteries potentially offers major mechanistic benefits compared to other anode contenders and battery systems, such as lithium metal in solid-state architectures or alloys in liquid-electrolyte batteries. This perspective discusses key advantages of alloy anode materials for solid-state batteries, including the avoidance of the short circuiting observed with lithium metal and the chemo-mechanical stabilization of the solid-electrolyte interphase (SEI). We further discuss open research questions and challenges in engineering alloy-anode-based solid-state batteries, with the goal of advancing our understanding and control of alloy anode materials within solid-state architectures toward commercial application.

KEYWORDS

Alloy anodes, solid-state batteries, energy storage, chemo-mechanics

Introduction

Solid-state batteries (SSBs) have emerged as an important technology for powering future electric vehicles and other applications due to their potential for enhanced safety and higher energy content compared to Li-ion batteries.[1-3] The development of SSBs has been accelerated by the discovery of new solid-state electrolyte (SSE) materials with high Li^+ conductivity (>10^{-3} S cm^{-1}), making them competitive with liquid electrolytes.[4, 5] A key aspect of the promise of SSBs is that the all-solid-state architecture could provide mechanistic advantages to enable the reliable use of high-capacity electrode materials beyond those used in Li-ion batteries.[3] As an example of a next-generation electrode material that could be enabled within SSBs, lithium metal anodes have received considerable research and development attention.[6, 7] Lithium metal has the highest theoretical charge storage capacity (3861 mAh g^{-1}) of all anode candidates and is thought to exhibit more stable interfaces in contact with certain SSEs compared to liquid electrolytes.[8, 9] Indeed, lithium metal anodes paired with high-capacity intercalation cathodes can allow for stack-level energy density greater than 1,100 Wh L^{-1} and specific energy approaching 400 Wh kg^{-1}, as shown in Fig. 1A. While substantial progress has been made in the development of lithium metal anodes, reliably controlling the lithium electrodeposition/stripping process at solid-state electrochemical interfaces has proven to be much more challenging than was initially envisioned.[8, 10-14] In particular, the growth of lithium filaments to form short circuits and the loss of contact at interfaces remain difficult challenges to solve.

Recently, there has been growing interest in investigating other types of high-capacity anode materials for SSBs. In particular, materials that alloy with Li ("alloy anodes") have shown promising electrochemical behavior in SSBs,[15-22] and they are also being commercially pursued by companies such as Solid Power.[23] Alloy anode materials, such as silicon, tin, aluminum, and others, can store more Li per mass and volume than conventional graphite anodes,[24-27] and their use in SSBs can therefore enable specific energy and energy density values much higher than conventional Li-ion batteries (Fig. 1A). The predicted energy density values of ~1,000 – 1,200 Wh L^{-1} for alloy-based SSBs are similar to those predicted for lithium metal SSBs when excess lithium is used (as is often the case), but alloy-based cells have lower specific energies (Fig. 1A). Alloy anodes have other benefits compared to lithium, as they can avoid many of the degradation modes associated with the use of lithium metal in SSBs, including dendrite growth that causes short

circuiting. However, the relatively large volumetric and structural changes in alloy materials during charge/discharge can cause material degradation.[28] Even if lithium metal-based SSBs are successfully commercialized, SSBs with varying electrode chemistries will likely be of interest for different use cases, and successful development of multiple electrode material options is thus a high priority.

Alloy anodes are not new; indeed, they have been investigated since the early days of Li-ion battery development.[29-32] Table 1 includes a list of selected alloy materials and their electrochemical, volume change, and transport properties. The last 15 years have seen major research efforts dedicated to replacing graphite anodes in liquid-electrolyte Li-ion batteries with alloy materials such as silicon,[33-36] with extensive work at the research scale and in industry dedicated to understanding reaction mechanisms and engineering complex material structures for long-term stability. Steady progress over the years has led to recent commercial advances, such as Sila Nanotechnologies' incorporation of silicon into commercial anodes for Li-ion batteries with ~20 % higher energy density than comparable graphite cells.[37] However, the energy storage community has not yet been able to develop cells that take advantage of the full capabilities of alloy anodes, since silicon is usually incorporated as a minor component instead of as the dominant material in the composite electrode.

The challenges of using alloy materials to reliably deliver high capacity with minimal degradation during charge/discharge cycling arise largely because of the chemo-mechanical interactions of these materials with their surroundings within a battery system. The all-solid environment in SSBs presents entirely new interfacial interactions and chemo-mechanical behavior compared to conventional liquid environments, which could allow for improved cycling performance of alloy anodes while avoiding deleterious shorting issues when using lithium metal. As research on alloy anodes for SSBs has only recently begun to accelerate, this Perspective article is meant to introduce possible benefits and challenges associated with the use of alloy anodes in SSBs, with the intention of spurring further research towards advancing the science and technology of alloy-anode-based SSBs.

Table 1. Electrochemical, volume change, and transport properties of various lithium alloy materials.

Alloy	Most Lithiated Phase	Specific Capacity (mAh g^{-1})	Average Potential vs. Li/Li^+ (V)	Volume Change (%)	Li Diffusion Coefficient ($cm^2 s^{-1}$)
Si	$Li_{15}Si_4$ [38]	3579 [39]	0.4 [39]	320 [40]	10^{-11}-10^{-13} [41-43, a]
Sn	$Li_{4.4}Sn$ [39]	993 [39]	0.50 [39]	260 [40]	10^{-14}-10^{-16} [44, a]
Al	LiAl [39]	990 [39]	0.38 [39]	96 [40]	10^{-9}-10^{-11} [45, 46, a]
Sb	Li_3Sb [39]	660 [39]	0.95 [39]	200 [40]	10^{-8}-10^{-9} [47]
In	$Li_{13}In_3$ [48]	1012 [39]	0.3 [39]	105 [49, c]	~10^{-8} [50]
Mg	Li_3Mg [40]	3350 [40]	0.03 [39]	100 [40]	10^{-7} [51, b]
Zn	LiZn [27]	410 [39]	0.38 [39]	98 [24]	10^{-8}-10^{-10} [52, 53, a]

[a] *Measured across multiple phases*
[b] *Measured for the most-lithiated phase*
[c] *Measured for the LiIn phase*

Benefits of Alloy Anodes for Solid-State Batteries

In this section, we first explore the predicted energy density/specific energy of alloy-anode based SSBs, and then we discuss expected mechanistic advantages of the use of alloys in solid-state environments compared to their use in liquids, as well as compared to other anode materials for SSBs.

Energy metrics. A major impetus for research and development of alloy-anode-based SSBs is their predicted high energy density and specific energy, as already mentioned. Figure 1A shows the theoretical energy density and specific energy values for a variety of different solid-state and liquid-based cell stacks (see the Supplemental Information for details on calculations). These calculated values pair different anodes with high-capacity $LiNi_{0.8}Mn_{0.1}Co_{0.1}O_2$ (NMC811) composite cathodes using an N:P (negative to positive) ratio of 1.1, and they take into account current collectors, separator, and electrode mass/volume but not external packaging. Figure 1B shows a schematic of a cell stack used for the calculations, in which the SSE material is included in the cathode composite, as the 20-μm thick separator, and in some cases in the anode composite.

There are two clusters of values from SSBs with alloy anodes in Fig. 1A, highlighted in green and blue. These two clusters arise when using two different exemplary SSE materials within the cells; the blue cluster with lower specific energy utilizes the oxide $Li_7La_3Zr_2O_{12}$ (LLZO), and the green cluster with higher specific energy utilizes the sulfide Li_6PS_5Cl (LPSC). The lower specific energy of LLZO-based cells in Fig. 1 results from the high density of LLZO, and removing

LLZO from the cathode composite would boost specific energy substantially (not shown in Fig. 1A). Figure 1A also shows that Li_6PS_5Cl-based SSBs have slightly lower specific energy (but similar energy density) compared to equivalent liquid-electrolyte cells; this is again because this SSE has higher density than liquid electrolytes, and these specific energy differences could be minimized by including less SSE in the composite cathode. Overall, it is clear that using SSE materials with low density and minimizing the use of SSE materials within the electrode structures are key strategies for achieving maximal specific energy. In all cases, however, alloy anode-based SSBs with the Li_6PS_5Cl solid electrolyte exceed the energy density and specific energy of the graphite-based liquid-electrolyte Li-ion cell included for comparison in Fig. 1A.

We next focus on the effects of different alloy anode materials on energy metrics. Within the green oval representing Li_6PS_5Cl-based SSBs in Fig. 1A, individual points representing SSBs with aluminum (990 mAh g^{-1}), tin (993 mAh g^{-1}), and silicon (3579 mAh g^{-1}) are shown. The circular data points assume the anode structures include 40 vol % SSE, and the triangular points assume that the anode is made of pure alloy material. While silicon-based anodes result in the highest specific energy and energy density, the differences among cells with various active materials are relatively small despite their large differences in specific capacity. This is because of the diminishing returns in terms of stack-level metrics for anode specific capacities greater than ~1000 mAh g^{-1},[54, 55] since the cells must still contain the same amount of cathode material. This trend is expected among other alloys as well. Another conclusion from comparing the values in Fig. 1A is that the inclusion of SSE material within an alloy anode composite (circles) does not significantly reduce the energy values compared to a pure anode material (triangles). This is largely because the alloy electrodes are relatively thin compared to the cathode as a result of the higher Li storage capacities of the alloy materials, and thus adding SSE to the anode requires only a minimal amount of additional material in comparison to the rest of the cell stack.

Lithium-metal based cells using SSEs and liquid electrolytes exhibit the highest specific energy in Fig. 1A. Interestingly, though, the true energy advantage of lithium is achieved in an "anode-free" configuration, where all lithium is plated on a bare current collector during the first charge. While such a concept is promising, it is challenging to achieve stable cycling with anode-free cells (using either liquid or solid electrolytes) for several reasons, including because of the extremely high Coulombic efficiencies required and zero excess Li^+ inventory. When 1× excess lithium is used (i.e., a ~20-μm lithium foil is used as the anode), the energy density of the cell is

similar to the alloy anode cells, while still surpassing alloy anodes in specific energy. We note that in all cases for lithium or alloy anodes, the metrics in Fig. 1A are calculated in the discharged state, and the necessary net volume increase in the cell after charge would result in lower energy density when calculated in the charged state.

Overall, these metrics make it clear that alloy-anode-based SSBs exceed the energy density and specific energy of conventional Li-ion batteries and could approach the energy density of lithium-metal-based cells, but the details of material and composite electrode engineering in the anode, separator, and cathode play important roles that can significantly affect these values. Additionally, further energy advantages not captured in Fig. 1A are expected for SSBs compared to Li-ion cells, such as the possibility of bipolar stacking of electrodes in which the cathode and anode are coated onto either side of the same current collector. This could enable a reduction in the volume of current collectors and packaging, which would substantially enhance energy density for SSBs compared to the estimates in Fig. 1, which do not take into account such effects.[56] As a final note, the predicted metrics in Fig. 1 assume an N:P ratio of 1.1, which contrasts with the widespread use of thick alloy anode foils (such as indium) in research demonstrations of SSBs with the primary purpose of acting as a counter electrode while avoiding the difficulties of using a lithium metal electrode. Such thick foils have large excess capacity that makes electrochemical comparison to cells with realistic N:P ratios impossible, and the energy advantages shown in Fig. 1 are only present when much thinner alloy anodes are used.

Solid-electrolyte interphase (SEI). The SEI in liquid-electrolyte Li-ion batteries is a film that grows on the anode surface due to electrochemical instability of the liquid electrolyte at the low electrode potential of the anode (< ~1 V vs Li/Li^+).[57, 58] In Li-ion batteries with a graphite anode, the SEI film grows to a thickness of 10-50 nm and plays an important role in charge transfer.[59] Alloy anodes used in liquid electrolytes are notorious for exacerbating and accelerating SEI growth, which consumes Li^+ and electrolyte solvent, leading to high cell impedance and eventual failure (Fig. 2A).[60-62] Excessive SEI growth occurs because of the cyclic changes of the surface dimensions of the alloy particles during lithiation/delithiation, which can fracture already-formed SEI and expose new surfaces for SEI to grow upon.[63] Engineering efforts to mitigate this issue for liquid-electrolyte cells have primarily involved fabricating hollow or composite alloy structures[34, 64, 65] that can accommodate volume changes while retaining approximately constant

outer surface dimensions. Such structures, however, can result in low tap density and reduced energy density.

The all-solid-state nature of SSBs presents entirely different interfacial dynamics: at the interface between an alloy active material and an SSE, the SSE does not flow to continually wet the alloy material surface during volume changes, and it is thus possible that this will result in reduced extent of SEI formation compared to alloys in liquid electrolytes (Fig. 2B).[18, 20, 66] Furthermore, the chemical and structural transformations during SEI formation in SSEs are fundamentally different than in liquid electrolytes,[9, 67-69] and some SSEs are known to form kinetically stabilized interphases at low potentials.[70] These ideas suggest that it may be easier to achieve stable long-term cycling of alloy anodes in solid-state environments without complicated structuring of active materials, as supported by recent studies reporting good cyclability of micron-sized alloy particles.[15, 16] These concepts require further investigation to understand completely.

Comparison to lithium metal: short circuiting and interfacial contact loss. The lithium metal anode has received enormous attention for SSBs because of its high specific capacity and the theory that mechanically stiff SSEs could prevent detrimental lithium filament or dendrite growth.[71] While important progress has been made in understanding and improving lithium electrodeposition/stripping behavior at SSE interfaces,[7] the twin problems of lithium filament growth and interfacial contact loss remain. Lithium filament growth through the SSE to form short circuits in cells is particularly insidious and pervasive (Fig. 2C);[10, 11, 72] this process is not completely understood but is thought to involve fracture of the SSE followed by filling of the crack(s) with lithium.[73-75] Filaments have also been detected to grow along grain boundaries and through porosity within SSEs.[10, 76, 77] Likewise, loss of contact between lithium and the SSE during stripping is difficult to avoid[8, 14] and can hasten lithium filament growth by causing high local current densities.[13, 78] The use of a "host" material (such as alloys or graphite) to contain Li can bypass the problems of lithium metal filament growth and interfacial contact loss in SSBs, since the host provides stable sites for Li insertion/removal while maintaining physical/electrical contact and preventing lithium metal growth. We note, of course, that the use of host materials for Li storage is a fundamental tenet of Li-ion batteries, but alloy hosts have not been widely investigated for SSBs despite their promising characteristics. This is perhaps due to the field's overriding recent focus on lithium metal anodes for SSBs.

In addition to the benefits of pure alloy anodes, a number of studies have shown positive impacts of using alloys to affect and control lithium deposition/stripping dynamics for lithium metal anodes; we emphasize that these studies focus on lithium metal anodes and only use minimal alloy material in attempts to improve lithium metal behavior.[79-82] For instance, silver particles included in a carbon composite were used as an electrode for solid-state deposition of lithium over hundreds of cycles, in which the silver reportedly migrated through the electrode during charge/discharge.[83] Other alloy metals such as magnesium exhibit high Li diffusivity (Table 1), which has been demonstrated to be useful for ensuring sufficient Li supply to the interface during lithium stripping to prevent void formation.[84] While these strategies are promising, lithium metal degradation modes can still persist, and thus this is a fundamentally different approach compared to using solely alloy materials as the anode host.

Chemo-mechanics. Alloy anode materials undergo 50-300 % volume change during lithiation/delithiation (Table 1),[55, 85] which is much larger than conventional intercalation materials. There is also a net volume change of the cell stack when used in conjunction with cathode materials such as $LiNi_{0.8}Co_{0.1}Mn_{0.1}O_2$, since the partial molar volumes of Li^+ in the cathode and anode are different.[55, 86] In liquid-cell batteries, material expansion at the anode during charge can largely be accommodated by flow of the liquid electrolyte, but in SSBs, expansion can generate and transmit stress and strain throughout the cell stack.[16, 49, 87-89] While this may cause problems, such as mechanical degradation or delamination[69] (see next section), it also brings about the possibility of controlling the global and local chemo-mechanical environments experienced by alloy materials during reactions. Depending on cell design, the stack pressure applied to a SSB can be transmitted to the electrode materials, which may be able to help control or direct the morphology changes of alloy materials during reactions. Furthermore, there is a potential opportunity to take advantage of rigid cell designs to cause compressive stress to be intrinsically generated within an anode during lithiation (volume expansion), which may enhance material durability.

Electrode design and manufacturing. Particulate alloy materials can be incorporated into slurry-cast or dry-cast composite electrodes,[15] similarly to graphite or other active materials. In contrast to graphite, though, many alloy anode materials can also be manufactured directly as metallic foils. This opens the exciting possibility of doing away with slurry-casting completely and instead directly fabricating metal foil anodes for incorporation into SSBs, which would likely

reduce costs and the environmental impact of slurry solvent recycling.[48, 90-92] While such an approach gives rise to questions of whether ion conduction rates through the electrode are sufficient, recent work on Si-based anodes for SSBs shows that it is possible to use a virtually pure Si anode with only a minute amount of binder under realistic cycling conditions,[15] providing support for this idea.

Research Questions and Challenges

Chemo-mechanics. A prevailing scientific question associated with the use of alloy anodes in SSBs is whether the volumetric and structural changes that occur during each cycle can be controlled either in composite or pure electrodes to maintain connectivity at solid-solid electrochemical interfaces. Research is needed to understand the dynamic chemical and mechanical interactions of alloy anode materials with various SSE materials. Expansion of alloy particles or structures can cause stress and strain generation, as investigated with *in situ* stress measurements in prior work.[16] These effects may cause local yielding of soft SSEs such as sulfides. Furthermore, alloy anode materials feature mechanical properties that strongly vary with their composition, in contrast to the invariant mechanical properties of lithium metal anodes. Prior experiments on silicon and tin have shown that the yield strength and Young's modulus decrease significantly from the pure material to the fully lithiated alloy;[93, 94] for instance, silicon's yield strength decreases from ~2 GPa to ~430 MPa upon full lithiation.[95] Furthermore, it is possible that the mechanisms governing plastic deformation change from low to high Li content. These changing properties have important implications for the use of alloys in SSBs, as the plastic deformation and yielding behavior can change with state of charge, which could affect structural and morphological evolution of the anode. Further understanding of the relationships between mechanical properties and alloy anode evolution in SSBs, as well as measurement of mechanical properties of alloys beyond silicon and tin, are needed.

A related important aspect of the use of alloys in SSBs is the role of applied stack pressure on material and interfacial evolution[88] – how does the magnitude of the stack pressure affect local stresses at interfaces, interfacial connectivity, and deformation of alloy materials with cycling? Many studies in the literature on both lithium metal and alloy electrodes use very high stack pressures up to 250 MPa,[77, 96, 97] but relatively low stack pressures (~1 MPa) are thought to be

needed for realistic SSB devices.[1] The yield strengths of fully-lithiated alloy materials are much higher than pure lithium metal; for instance, the yield strength of fully-lithiated silicon is ~430 MPa,[95] while that for bulk lithium is ~1 MPa.[98, 99] Thus, while moderate stack pressures can cause yielding of lithium electrodes to maintain contact at interfaces, this is likely not the case for alloys. However, alloying reactions themselves generate high internal stresses that cause internal yielding and deformation of the material,[100] and it is possible that an externally applied stack pressure could "bias" this intrinsic deformation to influence the morphological evolution of the anode. In short, it is necessary to understand and report the effects of a range of stack pressures (including low stack pressures) on the evolution of material morphology, contact at interfaces, and electrochemical behavior of alloy anodes. One route to reduce required stack pressures may be to encapsulate alloy particles in a softer matrix, such as an ion-conducting polymer with low interfacial impedance in contact with alloys, that deforms more easily to retain interfacial contact. In general, finding ways to reduce the external stack pressure applied to alloy-based cells is critical for commercial feasibility.

As shown in Fig. 3, realistic SSBs with alloy (or other) anodes require thin SSE separators to achieve high specific energy and energy density; 20 μm is targeted, with further thinning advantageous. The vast majority of research demonstrations of SSBs, however, utilize much thicker SSE pellets (0.5 – 1 mm), although there have been recent efforts toward developing thin separators.[101] Such thin separators may exhibit different chemo-mechanical responses to electrode volume changes. Research effort is thus needed to understand the mechanical stability of such separators under various mechanical constraint conditions during the extreme and potentially non-uniform volume changes of alloy anodes.

Electron/ion transport and electrode/cell design. A key aspect of electrode design for SSBs is the need for ion and electron transport pathways within the electrode to support sufficient ion/electron transport rates to enable fast charge and discharge.[102] The US Department of Energy long-term fast-charge target is to deliver 200 miles of electric vehicle range in 7.5 min.[103, 104] The lack of a liquid electrolyte in SSBs means that either a solid ion-conducting phase must be included in the electrode structure, or that the active material and/or other phases within an electrode must exhibit sufficiently high ion diffusion rates. Many SSB electrodes developed in the research literature (both anodes and cathodes) have consisted of a composite mixture of the active material, an SSE material, and potentially other additives (binders or electronically conductive additives).[105]

An advantage of many alloy anodes is that they are intrinsically electronically conductive, making electron-conducting additives unnecessary. Ion conduction is potentially a larger problem, however. While many highly lithiated metals exhibit relatively high Li diffusivities (see Table 1),[45, 47] the active mass loadings needed to enable high-energy density batteries (3-4 mAh cm^{-2}) can necessitate fairly thick electrodes, which may require SSE materials to be incorporated within the electrode composites to achieve high charge/discharge rates. The incorporation of inactive SSE materials into an electrode composite can reduce the volumetric charge storage, which is a problem both for anode and cathode composites.[106] Figure 3A-B show the calculated specific energy and energy density for silicon-based SSBs as a function of the silicon volume fraction in the anode composite (as well as the SSE separator thickness), assuming the use of the NMC-811 composite cathode identical to the calculations for Fig. 1. Energy density is more affected than specific energy by the anode active material volume fraction.

Creative electrode design to enable sufficient ion transport with minimal additives, perhaps by taking advantage of structured ion transport pathways or fast surface diffusion, is an important research direction both for anodes and cathodes. Furthermore, diffusion rates of Li in alloys can vary by orders of magnitude with state of charge[107] (Table 1), giving rise to important fundamental questions regarding how the spatio-temporal evolution of diffusivity is linked to reaction behavior in alloy electrodes, and suggesting that electrode design to include high-diffusivity phases could enable fast charge/discharge behavior. The recent work by Tan *et al.* showing cycling of almost pure Si electrodes suggests that at least some alloy anodes can operate without ion-conducting additives,[15] but it is not clear under which conditions this is true or which materials are appropriate.

SEI growth. As previously discussed, the solid-solid electrochemical interface may present advantages in terms of curtailing excess SEI growth at alloy anode interfaces compared to liquid electrolytes, which is an advantage of using alloy anodes in SSBs. Although this could be true, we have only limited knowledge of interphase structure, chemistry, and evolution in SSEs in contact with alloy anodes. Significant progress has been made in the SSB field in recent years in understanding reductive instabilities of various SSE materials,[68] and the effects of electron conduction through an interphase on the extent of further growth have been well-documented.[108] However, these efforts have primarily been focused on lithium metal/SSE interfaces, and lithium metal has a lower electrode potential than alloys of interest, which could contribute to different

phases that form at interfaces as well as different interphase growth kinetics.[109] The effects of such factors on electrochemical behavior and stability for alloy electrodes require further investigation.

Conclusion

The exceedingly attractive Li storage capacities of alloys have long driven efforts to incorporate them into high energy, durable rechargeable batteries. These efforts have recently begun to bear fruit for conventional liquid-cell Li-ion batteries, in which engineered alloy materials are being incorporated with increasing fractional quantities to boost energy storage capabilities. However, the fundamental characteristics of the dynamic alloy/liquid electrolyte interface have given rise to substantial roadblocks in achieving long-term cycling stability of alloy anodes. Solid-state batteries with alloy anodes offer the intriguing possibility of achieving long-term stability and high energy density due to the different properties of the solid-solid electrochemical interface. Even with the likely development of high-energy SSBs with lithium metal anodes, alloy-anode-based SSBs are still attractive due to their improved resistance to short circuiting, potential for long-term stability, and better energy metrics than graphite anodes. To realize this promise, however, fundamental and applied work is needed to advance our understanding and control over the evolution of alloy materials within SSBs. Given the vast need for improved energy storage solutions and the variety of applications and use cases that may benefit from different battery chemistries, the development of alloy-anode-based SSBs appears to be an urgent priority.

ACKNOWLEDGMENTS

J.A.L. acknowledges support from a NASA Space Technology Research Fellowship. K.A.C. acknowledges support from a NASA Space Technology Graduate Research Opportunities (NSTGRO) Award. Support is acknowledged from NASA Grant Number 80NSSC21M0101.

AUTHOR CONTRIBUTIONS

J.A.L. – Methodology, Formal Analysis, Writing, Visualization. K.A.C. – Writing. Y. L. – Writing. M.T.M. – Conceptualization, Formal Analysis, Writing, Visualization, Supervision.

DECLARATION OF INTERESTS

M.T.M. and Y.L. are inventors on a provisional patent related to solid-state batteries.

REFERENCES

1. Albertus, P., et al. (2021). Challenges for and pathways toward Li-metal-based all-solid-state batteries. ACS Energy Lett. *6*, 1399-1404.
2. Janek, J., and Zeier, W. G. (2016). A solid future for battery development. Nat. Energy *1*, 16141.
3. Wang, M. J., Kazyak, E., Dasgupta, N. P., and Sakamoto, J. (2021). Transitioning solid-state batteries from lab to market: Linking electro-chemo-mechanics with practical considerations. Joule *5*, 1371-1390.
4. Famprikis, T., Canepa, P., Dawson, J. A., Islam, M. S., and Masquelier, C. (2019). Fundamentals of inorganic solid-state electrolytes for batteries. Nat. Mater. *18*, 1278-1291.
5. Bachman, J. C., Muy, S., Grimaud, A., Chang, H.-H., Pour, N., Lux, S. F., Paschos, O., Maglia, F., Lupart, S., Lamp, P., Giordano, L., and Shao-Horn, Y. (2016). Inorganic solid-state electrolytes for lithium batteries: Mechanisms and properties governing ion conduction. Chem. Rev. *116*, 140-162.
6. Hatzell, K. B., Chen, X. C., Cobb, C. L., Dasgupta, N. P., Dixit, M. B., Marbella, L. E., McDowell, M. T., Mukherjee, P. P., Verma, A., Viswanathan, V., Westover, A. S., and Zeier, W. G. (2020). Challenges in lithium metal anodes for solid-state batteries. ACS Energy Lett. *5*, 922-934.
7. Krauskopf, T., Richter, F. H., Zeier, W. G., and Janek, J. (2020). Physicochemical concepts of the lithium metal anode in solid-state batteries. Chem. Rev. *120*, 7745-7794.
8. Krauskopf, T., Hartmann, H., Zeier, W. G., and Janek, J. (2019). Toward a fundamental understanding of the lithium metal anode in solid-state batteries-an electrochemo-mechanical study on the garnet-type solid electrolyte $Li_{6.25}Al_{0.25}La_3Zr_2O_{12}$. ACS Appl. Mater. Interfaces *11*, 14463-14477.
9. Wenzel, S., Sedlmaier, S. J., Dietrich, C., Zeier, W. G., and Janek, J. (2018). Interfacial reactivity and interphase growth of argyrodite solid electrolytes at lithium metal electrodes. Solid State Ionics *318*, 102-112.
10. Cheng, E. J., Sharafi, A., and Sakamoto, J. (2017). Intergranular Li metal propagation through polycrystalline $Li_{6.25}Al_{0.25}La_3Zr_2O_{12}$ ceramic electrolyte. Electrochim. Acta *223*, 85-91.
11. Kazyak, E., Garcia-Mendez, R., LePage, W. S., Sharafi, A., Davis, A. L., Sanchez, A. J., Chen, K.-H., Haslam, C., Sakamoto, J., and Dasgupta, N. P. (2020). Li penetration in ceramic solid electrolytes: Operando microscopy analysis of morphology, propagation, and reversibility. Matter *2*, 1025-1048.
12. Spencer Jolly, D., Ning, Z., Hartley, G. O., Liu, B., Melvin, D. L. R., Adamson, P., Marrow, J., and Bruce, P. G. (2021). Temperature dependence of lithium anode voiding in argyrodite solid-state batteries. ACS Appl. Mater. Interfaces *13*, 22708-22716.
13. Kasemchainan, J., Zekoll, S., Spencer Jolly, D., Ning, Z., Hartley, G. O., Marrow, J., and Bruce, P. G. (2019). Critical stripping current leads to dendrite formation on plating in lithium anode solid electrolyte cells. Nat. Mater. *18*, 1105-1111.

14. Lewis, J. A., et al. (2021). Linking void and interphase evolution to electrochemistry in solid-state batteries using operando X-ray tomography. Nat. Mater. *20*, 503-510.
15. Tan, D., H. S., et al. (2021). Carbon-free high-loading silicon anodes enabled by sulfide solid electrolytes. Science *373*, 1494-1499.
16. Han, S. Y., Lee, C., Lewis, J. A., Yeh, D., Liu, Y., Lee, H.-W., and McDowell, M. T. (2021). Stress evolution during cycling of alloy-anode solid-state batteries. Joule *5*, 2450-2465.
17. Yamamoto, M., Terauchi, Y., Sakuda, A., and Takahashi, M. (2018). Slurry mixing for fabricating silicon-composite electrodes in all-solid-state batteries with high areal capacity and cycling stability. J. Power Sources *402*, 506-512.
18. Maresca, G., Tsurumaki, A., Suzuki, N., Yoshida, K., Panero, S., Aihara, Y., and Navarra, M. A. (2021). Sn/C composite anodes for bulk-type all-solid-state batteries. Electrochim. Acta *395*, 139104.
19. Kim, J. Y., Jung, S., Kang, S. H., Park, J., Lee, M. J., Jin, D., Shin, D. O., Lee, Y.-G., and Lee, Y. M. (2022). Graphite–silicon diffusion-dependent electrode with short effective diffusion length for high-performance all-solid-state batteries. Adv. Energy Mater. *12*, 2103108.
20. Cangaz, S., Hippauf, F., Reuter, F. S., Doerfler, S., Abendroth, T., Althues, H., and Kaskel, S. (2020). Enabling high-energy solid-state batteries with stable anode interphase by the use of columnar silicon anodes. Adv. Energy Mater. *10*, 2001320.
21. Afyon, S., Kravchyk, K. V., Wang, S., Broek, J. v. d., Hänsel, C., Kovalenko, M. V., and Rupp, J. L. M. (2019). Building better all-solid-state batteries with Li-garnet solid electrolytes and metalloid anodes. J. Mater. Chem. A *7*, 21299-21308.
22. Hänsel, C., Singh, B., Kiwic, D., Canepa, P., and Kundu, D. (2021). Favorable interfacial chemomechanics enables stable cycling of high-Li-content Li–In/Sn anodes in sulfide electrolyte-based solid-state batteries. Chem. Mater. *33*, 6029-6040.
23. How high-content silicon anodes can reshape the EV landscape. https://solidpowerbattery.com/high-content-silicon-anode/ (Accessed 2/5/2022).
24. Obrovac, M. N., and Chevrier, V. L. (2014). Alloy negative electrodes for Li-ion batteries. Chem. Rev. *114*, 11444-11502.
25. Choi, S., Kwon, T.-w., Coskun, A., and Choi, J. W. (2017). Highly elastic binders integrating polyrotaxanes for silicon microparticle anodes in lithium ion batteries. Science *357*, 279.
26. Nitta, N., Wu, F., Lee, J. T., and Yushin, G. (2015). Li-ion battery materials: Present and future. Mater. Today *18*, 252-264.
27. Nitta, N., and Yushin, G. (2014). High-capacity anode materials for lithium-ion batteries: Choice of elements and structures for active particles. Part. Syst. Characteriz. *31*, 317-336.
28. McDowell, M. T., Lee, S. W., Nix, W. D., and Cui, Y. (2013). 25th anniversary article: Understanding the lithiation of silicon and other alloying anodes for lithium-ion batteries. Adv. Mater. *25*, 4966-4985.
29. Dey, A. N. (1971). Electrochemical alloying of lithium in organic electrolytes. J. Electrochem. Soc. *118*, 1547.
30. Rao, B. M. L., Francis, R. W., and Christopher, H. A. (1977). Lithium-aluminum electrode. J. Electrochem. Soc. *124*, 1490-1492.
31. Wen, C. J., and Huggins, R. A. (1981). Chemical diffusion in intermediate phases in the lithium-silicon system. J. Solid State Chem. *37*, 271-278.
32. Wen, C. J., Boukamp, B. A., Huggins, R. A., and Weppner, W. (1979). Thermodynamic and mass transport properties of "LiAl". J. Electrochem. Soc. *126*, 2258-2266.

33. Magasinski, A., Dixon, P., Hertzberg, B., Kvit, A., Ayala, J., and Yushin, G. (2010). High-performance lithium-ion anodes using a hierarchical bottom-up approach. Nat. Mater. *9*, 353-358.
34. Liu, N., Lu, Z., Zhao, J., McDowell, M. T., Lee, H.-W., Zhao, W., and Cui, Y. (2014). A pomegranate-inspired nanoscale design for large-volume-change lithium battery anodes. Nat. Nanotechnol. *9*, 187.
35. Sung, J., Kim, N., Ma, J., Lee, J. H., Joo, S. H., Lee, T., Chae, S., Yoon, M., Lee, Y., Hwang, J., Kwak, S. K., and Cho, J. (2021). Subnano-sized silicon anode via crystal growth inhibition mechanism and its application in a prototype battery pack. Nat. Energy *6*, 1164-1175.
36. Chae, S., Choi, S.-H., Kim, N., Sung, J., and Cho, J. (2020). Integration of graphite and silicon anodes for the commercialization of high-energy lithium-ion batteries. Ang. Chem. Int. Ed. *59*, 110-135.
37. Sila nanotechnologies' Si anode enabling longer battery life in wearable electronics. https://arpa-e.energy.gov/news-and-media/blog-posts/arpa-e-investor-update-vol-5 (Accessed 2/5/2022).
38. Zhang, W.-J. (2011). Lithium insertion/extraction mechanism in alloy anodes for lithium-ion batteries. J. Power Sources *196*, 877-885.
39. Heligman, B. T., and Manthiram, A. (2021). Elemental foil anodes for lithium-ion batteries. ACS Energy Lett. *6*, 2666-2672.
40. Zhang, W.-J. (2011). A review of the electrochemical performance of alloy anodes for lithium-ion batteries. J. Power Sources *196*, 13-24.
41. Pharr, M., Zhao, K., Wang, X., Suo, Z., and Vlassak, J. J. (2012). Kinetics of initial lithiation of crystalline silicon electrodes of lithium-ion batteries. Nano Lett. *12*, 5039-5047.
42. Ding, N., Xu, J., Yao, Y. X., Wegner, G., Fang, X., Chen, C. H., and Lieberwirth, I. (2009). Determination of the diffusion coefficient of lithium ions in nano-Si. Solid State Ionics *180*, 222-225.
43. Xie, J., Imanishi, N., Zhang, T., Hirano, A., Takeda, Y., and Yamamoto, O. (2010). Li-ion diffusion in amorphous Si films prepared by RF magnetron sputtering: A comparison of using liquid and polymer electrolytes. Mater. Chem. Phys. *120*, 421-425.
44. Xie, J., Imanishi, N., Hirano, A., Takeda, Y., Yamamoto, O., Zhao, X. B., and Cao, G. S. (2010). Li-ion diffusion behavior in Sn, SnO and SnO_2 thin films studied by galvanostatic intermittent titration technique. Solid State Ionics *181*, 1611-1615.
45. Jow, T. R., and Liang, C. C. (1982). Lithium-aluminum electrodes at ambient temperatures. J. Electrochem. Soc. *129*, 1429-1434.
46. Armstrong, R. D., Brown, O. R., Ram, R. P., and Tuck, C. D. (1989). Lithium electrodes based upon aluminium and alloy substrates. i. Impedance measurements on aluminium. J. Power Sources *28*, 259-267.
47. Allcorn, E., Kim, S. O., and Manthiram, A. (2015). Lithium diffusivity in antimony-based intermetallic and FeSb–TiC composite anodes as measured by GITT. Phys. Chem. Chem. Phys. *17*, 28837-28843.
48. Han, S. Y., Lewis, J. A., Shetty, P. P., Tippens, J., Yeh, D., Marchese, T. S., and McDowell, M. T. (2020). Porous metals from chemical dealloying for solid-state battery anodes. Chem. Mater. *32*, 2461-2469.
49. Zhang, W., Schröder, D., Arlt, T., Manke, I., Koerver, R., Pinedo, R., Weber, D. A., Sann, J., Zeier, W. G., and Janek, J. (2017). (Electro)chemical expansion during cycling:

Monitoring the pressure changes in operating solid-state lithium batteries. J. Mater. Chem. A *5*, 9929-9936.
50. Hiratani, M., Miyauchi, K., Ito, Y., Kanehori, K., Kirino, F., and Kudo, T. Solid state lithium battery. US Patent No. 4,645,726, 1987.
51. Shi, Z., Liu, M., Naik, D., and Gole, J. L. (2001). Electrochemical properties of Li–Mg alloy electrodes for lithium batteries. J. Power Sources *92*, 70-80.
52. Anani, A., Crouch-Baker, S., and Huggins, R. A. (1987). Kinetic and thermodynamic parameters of several binary lithium alloy negative electrode materials at ambient temperature. J. Electrochem. Soc. *134*, 3098-3102.
53. Shi, Z., Liu, M., and Gole, J. L. (1999). Electrochemical properties of Li-Zn alloy electrodes prepared by kinetically controlled vapor deposition for lithium batteries. Electrochem. Solid-State Lett. *3*, 312.
54. Kasavajjula, U., Wang, C., and Appleby, A. J. (2007). Nano- and bulk-silicon-based insertion anodes for lithium-ion secondary cells. J. Power Sources *163*, 1003-1039.
55. Obrovac, M. N., Christensen, L., Le, D. B., and Dahn, J. R. (2007). Alloy design for lithium-ion battery anodes. J. Electrochem. Soc. *154*, A849.
56. Dixit, M., Parejiya, A., Essehli, R., Muralidharan, N., Haq, S. U., Amin, R., and Belharouak, I. (2022). SolidPAC is an interactive battery-on-demand energy density estimator for solid-state batteries. Cell Rep. Phys. Sci. *3*, 100756.
57. Heiskanen, S. K., Kim, J., and Lucht, B. L. (2019). Generation and evolution of the solid electrolyte interphase of lithium-ion batteries. Joule *3*, 2322-2333.
58. Wang, L., Menakath, A., Han, F., Wang, Y., Zavalij, P. Y., Gaskell, K. J., Borodin, O., Iuga, D., Brown, S. P., Wang, C., Xu, K., and Eichhorn, B. W. (2019). Identifying the components of the solid–electrolyte interphase in Li-ion batteries. Nat. Chem. *11*, 789-796.
59. Verma, P., Maire, P., and Novák, P. (2010). A review of the features and analyses of the solid electrolyte interphase in Li-ion batteries. Electrochim. Acta *55*, 6332-6341.
60. He, Y., et al. (2021). Progressive growth of the solid–electrolyte interphase towards the Si anode interior causes capacity fading. Nat. Nanotechnol. *16*, 1113-1120.
61. Corsi, J. S., Welborn, S. S., Stach, E. A., and Detsi, E. (2021). Insights into the degradation mechanism of nanoporous alloy-type Li-ion battery anodes. ACS Energy Lett. *6*, 1749-1756.
62. Huang, W., Wang, J., Braun, M. R., Zhang, Z., Li, Y., Boyle, D. T., McIntyre, P. C., and Cui, Y. (2019). Dynamic structure and chemistry of the silicon solid-electrolyte interphase visualized by cryogenic electron microscopy. Matter *1*, 1232-1245.
63. Wu, H., Chan, G., Choi, J. W., Ryu, I., Yao, Y., McDowell, M. T., Lee, S. W., Jackson, A., Yang, Y., Hu, L., and Cui, Y. (2012). Stable cycling of double-walled silicon nanotube battery anodes through solid–electrolyte interphase control. Nat. Nanotechnol. *7*, 310-315.
64. Li, S., Niu, J., Zhao, Y. C., So, K. P., Wang, C., Wang, C. A., and Li, J. (2015). High-rate aluminium yolk-shell nanoparticle anode for Li-ion battery with long cycle life and ultrahigh capacity. Nat. Commun. *6*, 7872.
65. Zhang, W.-M., Hu, J.-S., Guo, Y.-G., Zheng, S.-F., Zhong, L.-S., Song, W.-G., and Wan, L.-J. (2008). Tin-nanoparticles encapsulated in elastic hollow carbon spheres for high-performance anode material in lithium-ion batteries. Adv. Mater. *20*, 1160-1165.
66. Cervera, R. B., Suzuki, N., Ohnishi, T., Osada, M., Mitsuishi, K., Kambara, T., and Takada, K. (2014). High performance silicon-based anodes in solid-state lithium batteries. Energy Environ. Sci. *7*, 662-666.

67. Lewis, J. A., Cortes, F. J. Q., Boebinger, M. G., Tippens, J., Marchese, T. S., Kondekar, N., Liu, X., Chi, M., and McDowell, M. T. (2019). Interphase morphology between a solid-state electrolyte and lithium controls cell failure. ACS Energy Lett. *4*, 591-599.
68. Nolan, A. M., Zhu, Y., He, X., Bai, Q., and Mo, Y. (2018). Computation-accelerated design of materials and interfaces for all-solid-state lithium-ion batteries. Joule *2*, 2016-2046.
69. Ping, W., Yang, C., Bao, Y., Wang, C., Xie, H., Hitz, E., Cheng, J., Li, T., and Hu, L. (2019). A silicon anode for garnet-based all-solid-state batteries: Interfaces and nanomechanics. Energy Storage Mater. *21*, 246-252.
70. Ma, C., Cheng, Y., Yin, K., Luo, J., Sharafi, A., Sakamoto, J., Li, J., More, K. L., Dudney, N. J., and Chi, M. (2016). Interfacial stability of Li metal–solid electrolyte elucidated via in situ electron microscopy. Nano Lett. *16*, 7030-7036.
71. Monroe, C., and Newman, J. (2005). The impact of elastic deformation on deposition kinetics at lithium/polymer interfaces. J. Electrochem. Soc. *152*, A396.
72. Lewis, J. A., Lee, C., Liu, Y., Han, S. Y., Prakash, D., Klein, E. J., Lee, H.-W., and McDowell, M. T. (2022). Role of areal capacity in determining short circuiting of sulfide-based solid-state batteries. ACS Appl. Mater. Interfaces *14*, 4051-4060.
73. Ning, Z., et al. (2021). Visualizing plating-induced cracking in lithium-anode solid-electrolyte cells. Nat. Mater. *20*, 1121-1129.
74. Hao, S., Daemi, S. R., Heenan, T. M. M., Du, W., Tan, C., Storm, M., Rau, C., Brett, D. J. L., and Shearing, P. R. (2021). Tracking lithium penetration in solid electrolytes in 3D by in-situ synchrotron X-ray computed tomography. Nano Energy *82*, 105744.
75. Dixit, M. B., Singh, N., Horwath, J. P., Shevchenko, P. D., Jones, M., Stach, E. A., Arthur, T. S., and Hatzell, K. B. (2020). In situ investigation of chemomechanical effects in thiophosphate solid electrolytes. Matter *3*, 2138-2159.
76. Vishnugopi, B. S., Dixit, M. B., Hao, F., Shyam, B., Cook, J. B., Hatzell, K. B., and Mukherjee, P. P. (2022). Mesoscale interrogation reveals mechanistic origins of lithium filaments along grain boundaries in inorganic solid electrolytes. Adv. Energy Mater. *12*, 2102825.
77. Doux, J. M., Nguyen, H., Tan, D. H. S., Banerjee, A., Wang, X., Wu, E. A., Jo, C., Yang, H., and Meng, Y. S. (2019). Stack pressure considerations for room-temperature all-solid-state lithium metal batteries. Adv. Energy Mater. *10*, 1903253.
78. Wang, M. J., Choudhury, R., and Sakamoto, J. (2019). Characterizing the Li-solid-electrolyte interface dynamics as a function of stack pressure and current density. Joule *3*, 2165-2178.
79. Lu, Y., Huang, X., Ruan, Y., Wang, Q., Kun, R., Yang, J., and Wen, Z. (2018). An in situ element permeation constructed high endurance Li–LLZO interface at high current densities. J. Mater. Chem. A *6*, 18853-18858.
80. Dai, J., Yang, C., Wang, C., Pastel, G., and Hu, L. (2018). Interface engineering for garnet-based solid-state lithium-metal batteries: Materials, structures, and characterization. Adv. Mater. *30*, 1802068.
81. Fu, K., et al. (2017). Toward garnet electrolyte–based Li metal batteries: An ultrathin, highly effective, artificial solid-state electrolyte/metallic Li interface. Science Advances *3*, e1601659.
82. Kato, A., Suyama, M., Hotehama, C., Kowada, H., Sakuda, A., Hayashi, A., and Tatsumisago, M. (2018). High-temperature performance of all-solid-state lithium-metal batteries having Li/Li_3PS_4 interfaces modified with Au thin films. J. Electrochem. Soc. *165*, A1950-A1954.

83. Lee, Y.-G., et al. (2020). High-energy long-cycling all-solid-state lithium metal batteries enabled by silver–carbon composite anodes. Nat. Energy *5*, 299-308.
84. Krauskopf, T., Mogwitz, B., Rosenbach, C., Zeier, W. G., and Janek, J. (2019). Diffusion limitation of lithium metal and Li–Mg alloy anodes on LLZO type solid electrolytes as a function of temperature and pressure. Adv. Energy Mater. *9*, 1902568.
85. McDowell, M. T., Cortes, F. J. Q., Thenuwara, A. C., and Lewis, J. A. (2020). Toward high-capacity battery anode materials: Chemistry and mechanics intertwined. Chem. Mater. *32*, 8755-8771.
86. Koerver, R., Zhang, W., de Biasi, L., Schweidler, S., Kondrakov, A. O., Kolling, S., Brezesinski, T., Hartmann, P., Zeier, W. G., and Janek, J. (2018). Chemo-mechanical expansion of lithium electrode materials – on the route to mechanically optimized all-solid-state batteries. Energy Environ. Sci. *11*, 2142-2158.
87. Lee, C., Han, S. Y., Lewis, J. A., Shetty, P. P., Yeh, D., Liu, Y., Klein, E., Lee, H.-W., and McDowell, M. T. (2021). Stack pressure measurements to probe the evolution of the lithium–solid-state electrolyte interface. ACS Energy Lett. *6*, 3261-3269.
88. Piper, D. M., Yersak, T. A., and Lee, S.-H. (2012). Effect of compressive stress on electrochemical performance of silicon anodes. J. Electrochem. Soc. *160*, A77-A81.
89. Lewis, J. A., Tippens, J., Cortes, F. J. Q., and McDowell, M. T. (2019). Chemo-mechanical challenges in solid-state batteries. Trends Chem. *1*, 845-857.
90. Boles, S. T., and Tahmasebi, M. H. (2020). Are foils the future of anodes? Joule *4*, 1342-1346.
91. Heligman, B. T., Kreder, K. J., and Manthiram, A. (2019). Zn-Sn interdigitated eutectic alloy anodes with high volumetric capacity for lithium-ion batteries. Joule *3*, 1051-1063.
92. Kreder, K. J., Heligman, B. T., and Manthiram, A. (2017). Interdigitated eutectic alloy foil anodes for rechargeable batteries. ACS Energy Lett. *2*, 2422-2423.
93. Hertzberg, B., Benson, J., and Yushin, G. (2011). Ex-situ depth-sensing indentation measurements of electrochemically produced Si–Li alloy films. Electrochem. Commun. *13*, 818-821.
94. Hong, C. S., and Han, S. M. (2020). Mechanical properties of electrochemically lithiated Sn. Extreme Mech. Lett. *40*, 100907.
95. Berla, L. A., Lee, S. W., Cui, Y., and Nix, W. D. (2015). Mechanical behavior of electrochemically lithiated silicon. J. Power Sources *273*, 41-51.
96. Ye, L., and Li, X. (2021). A dynamic stability design strategy for lithium metal solid state batteries. Nature *593*, 218-222.
97. Zhou, L., Zuo, T.-T., Kwok, C. Y., Kim, S. Y., Assoud, A., Zhang, Q., Janek, J., and Nazar, L. F. (2022). High areal capacity, long cycle life 4 V ceramic all-solid-state Li-ion batteries enabled by chloride solid electrolytes. Nat. Energy *7*, 83-93.
98. Masias, A., Felten, N., Garcia-Mendez, R., Wolfenstine, J., and Sakamoto, J. (2019). Elastic, plastic, and creep mechanical properties of lithium metal. J. Mater. Sci. *54*, 2585-2600.
99. LePage, W. S., Chen, Y., Kazyak, E., Chen, K.-H., Sanchez, A. J., Poli, A., Arruda, E. M., Thouless, M. D., and Dasgupta, N. P. (2019). Lithium mechanics: Roles of strain rate and temperature and implications for lithium metal batteries. J. Electrochem. Soc. *166*, A89-A97.
100. McDowell, M. T., Ryu, I., Lee, S. W., Wang, C., Nix, W. D., and Cui, Y. (2012). Studying the kinetics of crystalline silicon nanoparticle lithiation with in situ transmission electron microscopy. Adv. Mater. *24*, 6034-6041.

101. Wang, C., Yu, R., Duan, H., Lu, Q., Li, Q., Adair, K. R., Bao, D., Liu, Y., Yang, R., Wang, J., Zhao, S., Huang, H., and Sun, X. (2022). Solvent-free approach for interweaving freestanding and ultrathin inorganic solid electrolyte membranes. ACS Energy Lett. *7*, 410-416.
102. Vishnugopi, B. S., Kazyak, E., Lewis, J. A., Nanda, J., McDowell, M. T., Dasgupta, N. P., and Mukherjee, P. P. (2021). Challenges and opportunities for fast charging of solid-state lithium metal batteries. ACS Energy Lett. *6*, 3734-3749.
103. Howell, D. *Enabling fast charging: A technology gap assessment*; US Department of Energy, Office of Energy Efficiency and Renewable Energy: October 2017, 2017.
104. Masias, A., Marcicki, J., and Paxton, W. A. (2021). Opportunities and challenges of lithium ion batteries in automotive applications. ACS Energy Lett. *6*, 621-630.
105. Randau, S., Weber, D. A., Kötz, O., Koerver, R., Braun, P., Weber, A., Ivers-Tiffée, E., Adermann, T., Kulisch, J., Zeier, W. G., Richter, F. H., and Janek, J. (2020). Benchmarking the performance of all-solid-state lithium batteries. Nat. Energy *5*, 259-270.
106. Dixit, M. B., Parejiya, A., Muralidharan, N., Essehli, R., Amin, R., and Belharouak, I. (2021). Understanding implications of cathode architecture on energy density of solid-state batteries. Energy Storage Mater. *40*, 239-249.
107. Wang, Z., Su, Q., Deng, H., and Fu, Y. (2015). Composition dependence of lithium diffusion in lithium silicide: A density functional theory study. ChemElectroChem *2*, 1292-1297.
108. Tippens, J., Miers, J. C., Afshar, A., Lewis, J. A., Cortes, F. J. Q., Qiao, H., Marchese, T. S., Di Leo, C. V., Saldana, C., and McDowell, M. T. (2019). Visualizing chemomechanical degradation of a solid-state battery electrolyte. ACS Energy Lett. *4*, 1475-1483.
109. Li, Y., Liu, M., Feng, X., Li, Y., Wu, F., Bai, Y., and Wu, C. (2021). How can the electrode influence the formation of the solid electrolyte interface? ACS Energy Lett. *6*, 3307-3320.

Figures

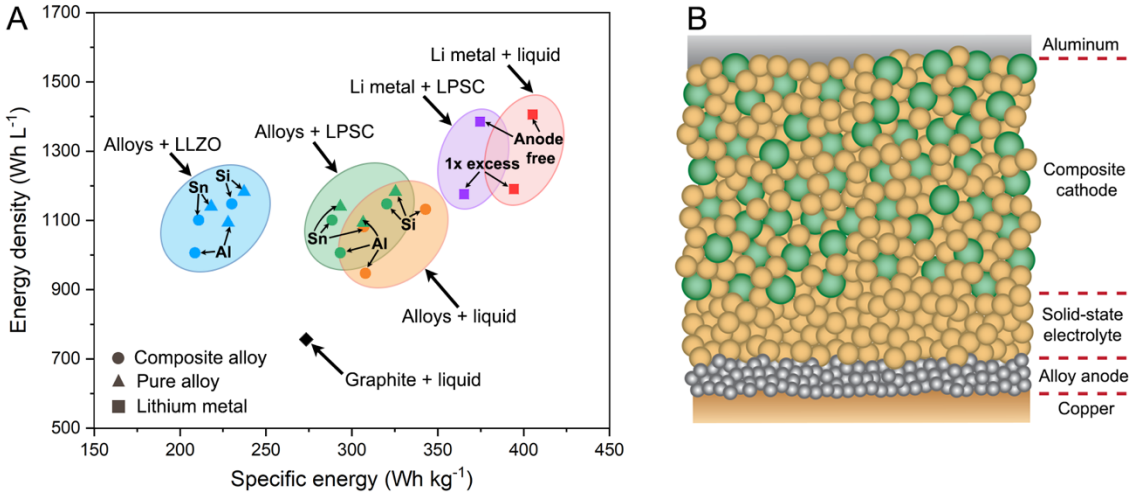

Figure 1. Analysis of the energy metrics alloy-anode-based SSBs compared to other battery chemistries.

(A) Predicted energy density (Wh L^{-1}) and specific energy (Wh kg^{-1}) of solid-state and liquid-based battery stacks with different anodes: graphite, lithium, and alloy materials (silicon, tin, and aluminum). For the alloy anodes, circles represent composite electrodes with the SSE material included in the electrode structure, while triangles represent the pure alloy anode material as the electrode. All cells assume pairing with a $LiNi_{0.8}Mn_{0.1}Co_{0.1}O_2$ (NMC811) composite cathode, and the SSB cells assume 40 vol% of the cathode architecture contains SSE material and that the SSE separator is 20 μm thick. LLZO = $Li_7La_3Zr_2O_{12}$; LPSC = Li_6PS_5Cl. See the Supplemental Information for full details on calculations. **(B)** Schematic of SSB material stack with an alloy anode considered for energy calculations.

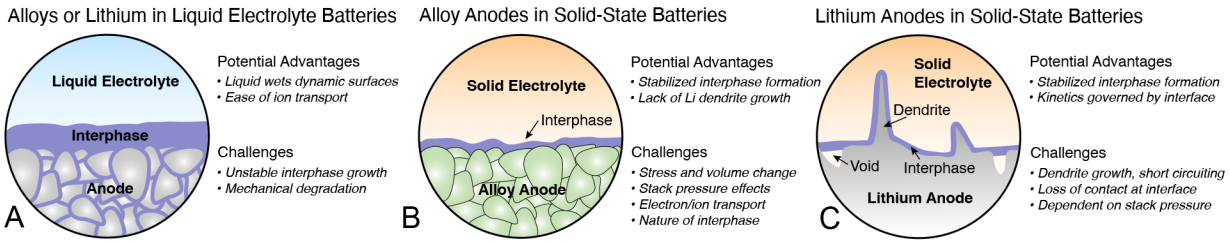

Figure 2. Mechanistic advantages and challenges of using alloy anodes in SSBs.

(A) Schematic of an alloy anode or lithium metal anode in a liquid electrolyte environment, along with potential advantages and challenges. **(B)** Schematic of an alloy anode used in a solid-state battery. **(C)** Schematic of a lithium metal anode used in a solid-state battery.

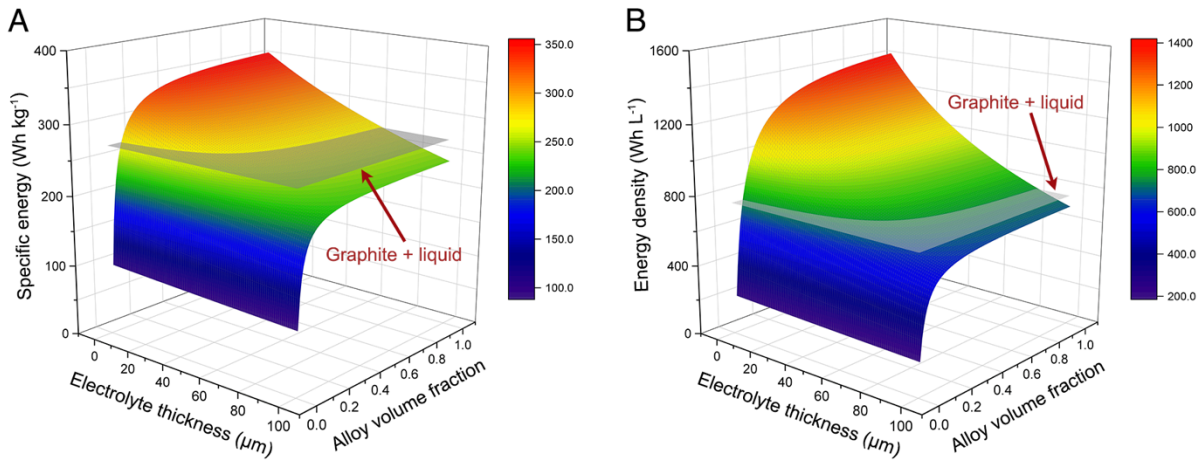

Figure 3. Effects of electrolyte thickness and alloy anode volume fraction on cell energy.

(A) Specific energy (Wh kg^{-1}) and **(B)** energy density (Wh L^{-1}) for a SSB stack as a function of the electrolyte separator thickness and the volume fraction of active material in the anode. The battery consists of silicon active anode material, Li_6PS_5Cl SSE in the anode, cathode, and separator, and NMC-811 active cathode material with 60 vol% active material loading in the cathode.

The specific energy and energy density for a single stack of materials (as shown in Fig. 1A) were calculated for different battery configurations as follows. First, assumptions were made regarding the areal capacities of each electrode. The cathode areal capacity was chosen to be 4.0 mAh cm^{-2}. The anode areal capacities were determined based on the use of an N:P ratio of 1.1 in most cases; these values are listed in Tables 1 and 2. The theoretical specific capacity and density values for each material that were used are listed in Table 3.

A volume ratio between the active material and electrolyte was assumed for each electrode evaluated; these ratios are listed in Tables 1 and 2. For the solid-state cells evaluated, it was assumed that each component containing SSE used the same type of SSE throughout the entire cell. Additionally, only active material and electrolyte were considered in the SSB composite electrodes. Calculations for composite electrodes in liquid cells assumed a composition of 95 wt% active material, 2.5 wt% binder, and 2.5 wt% conductive carbon. The porosity of each composite electrode with liquid electrolyte is listed in Table 2. A higher porosity was assumed for the alloy anodes due to their greater volume expansion during lithiation.

Using these compositions, the density of each composite electrode could be calculated by summing the material density (ρ_i) multiplied by the material volume fraction (ϕ_i) for each component in the composite.

$$\rho_{composite} = \sum_{i=1}^{N} \rho_i \phi_i \tag{1}$$

Given the active material's specific capacity (q_{active}), density (ρ_{active}), and volume fraction (ϕ_{active}), the electrode charge density (Q_{vol}) was then calculated using Equation 2.

$$Q_{vol} = q_{active} \rho_{active} \phi_{active} \tag{2}$$

The necessary electrode thickness ($l_{electrode}$) was then calculated by dividing the assumed areal capacity (Q_{areal}) by the electrode charge density.

$$l_{electrode} = \frac{Q_{areal}}{Q_{vol}} \tag{3}$$

The areal mass loading ($m_{electrode}$) of the electrode was calculated by multiplying the electrode thickness by the composite electrode density.

$$m_{electrode} = l_{electrode} \rho_{composite} \tag{4}$$

The entire thickness and areal mass loading of a single stack was calculated by summing the values of each individual component in the stack (Equations 5 and 6). Every stack used a 10 μm thick copper current collector and a 10 μm thick aluminum current collector. For Figure 1b, the thickness of the electrolyte layer was 20 μm in all cases. In Figure 3, the thickness of the electrolyte was intentionally varied to understand its effect on cell energy. The densities used to calculate the areal mass loadings for the current collectors and electrolyte are listed in Table 3.

$$l_{stack} = l_{Al} + l_{cathode} + l_{electrolyte} + l_{anode} + l_{Cu} \tag{5}$$

$$m_{stack} = m_{Al} + m_{cathode} + m_{electrolyte} + m_{anode} + m_{Cu} \tag{6}$$

With the total stack thickness and areal mass loading, the specific energy and energy density were calculated using equations 7 and 8. The assumed average cell voltages for each configuration are listed in Table 4, as well as the calculated energy values.

$$Specific\ energy = \frac{q_{cathode} V_{cell}}{m_{stack}} \tag{7}$$

$$Energy\ density = \frac{q_{cathode} V_{cell}}{l_{stack}} \tag{8}$$

Table 1. Composition (vol %) and areal capacity for each SSB electrode evaluated.

Composition (vol%)	**Areal capacity (mAh cm^{-2})**
60% $LiNi_{0.8}Mn_{0.1}Co_{0.1}O_2$, 40% LPSC	4.0
60% $LiNi_{0.8}Mn_{0.1}Co_{0.1}O_2$, 40% LLZO	4.0
60% Si, 40% LPSC	4.4
60% Al, 40% LPSC	4.4
60% Sn, 40% LPSC	4.4
60% Si, 40% LLZO	4.4
60% Al, 40% LLZO	4.4
60% Sn, 40% LLZO	4.4
100% Si	4.4
100% Al	4.4
100% Sn	4.4
1x excess Li (solid)	4.0
Anode free Li (solid)	0 (*in discharged state)

Table 2. Composition, areal capacity, and porosity for each liquid electrode evaluated.

Composition (wt%)	**Areal capacity (mAh cm^{-2})**	**Porosity (%)**
95% $LiNi_{0.8}Mn_{0.1}Co_{0.1}O_2$ 2.5% binder 2.5% conductive additive	4	30
95% graphite 2.5% binder 2.5% conductive additive	4.4	30
95% silicon 2.5% binder 2.5% conductive additive	4.4	50
95% aluminum 2.5% binder 2.5% conductive additive	4.4	50
95% tin 2.5% binder 2.5% conductive additive	4.4	50
1x excess Li (liquid)	4	-
Anode free Li (liquid)	0 (*in discharged state)	-

Table 3. List of the densities and specific capacities used.

Material	Density ($g\ cm^{-3}$)	Specific capacity ($mAh\ g^{-1}$)
Li_6PS_5Cl (LPSC)	1.86	-
$Li_7La_3Zr_2O_{12}$ (LLZO)	5.1	-
$LiNi_{0.8}Mn_{0.1}Co_{0.1}O_2$ (NMC)	4.78	200
Silicon	2.33	3579
Aluminum	2.7	990
Tin	7.27	992
Lithium	0.53	3861
Graphite	2.2	372
Binder	1.8	-
Conductive carbon	1.8	-
Liquid electrolyte	1.3	-
Aluminum	2.7	-
Copper	8.96	-

Table 4. Average voltage, specific energy, and energy density for each configuration analyzed.

	Average voltage (V)	Specific energy ($Wh\ kg^{-1}$)	Energy density ($Wh\ L^{-1}$)
Sulfides			
Li (1x excess)/LPSC/NMC	3.8	365	1176
Li (anodeless)/LPSC/NMC	3.8	375	1385
60% Si/LPSC/NMC	3.4	320	1147
60 % Al/LPSC/NMC	3.45	293	1006
60% Sn/LPSC/NMC	3.3	288	1101
100% Si/LPSC/NMC	3.4	325	1182
100% Al/LPSC/NMC	3.45	307	1094
100% Sn/LPSC/NMC	3.3	293	1140
Oxides			
60% Si/LLZO/NMC	3.4	230	1147
60% Al/LLZO/NMC	3.45	209	1006
60% Sn/LLZO/NMC	3.3	211	1101
100% Si/LLZO/NMC	3.4	237	1182
100% Al/LLZO/NMC	3.45	228	1094
100% Sn/LLZO/NMC	3.3	218	1140
Liquid			
Graphite/Liquid/NMC	3.7	274	756
Si/Liquid/NMC	3.4	343	1132
Al/Liquid/NMC	3.45	308	947
Sn/Liquid/NMC	3.3	307	1082
Li (1x excess)/Liquid/NMC	3.8	394	1191
Li (anodeless)/Liquid/NMC	3.8	405	1406